Dynamics of the Laguerre Gaussian $TEM^{*}_{0,l}$ mode in a solid-state laser

Y. F. Chen*
Department of Electrophysics, National Chiao Tung University, 1001 TA Hsueh Road, Hsinchu, Taiwan 30050, Republic of China

Y. P. Lan
Institute of Electro-Optical Engineering, National Chiao Tung University, Hsinchu, Taiwan 30050, Republic of China

(Received 21 November 2000; published 10 May 2001)

The dynamics of a solid-state laser sustaining the oscillation of the Laguerre–Gaussian $TEM^{*}_{0,l}$ mode is theoretically and experimentally studied. The results of investigations of the existence conditions of self-modulation, chaotic, frequency locking, and self-pulsing regimes are given. The experimental results, obtained using a diode-pumped solid-state laser, are well confirmed by the theoretical model. From the observations of the locking phenomena of the first-order family, we also confirm the theoretical predictions that the locking occurs as a subcritical bifurcation in a solid-state laser.

DOI: 10.1103/PhysRevA.63.063807 PACS number(s): 42.60.Mi, 42.65.Sf

I. INTRODUCTION

The recent rapid progress of diode-pumped microchip lasers has driven a renaissance of solid-state laser physics research and led to phenomena [1]. Fiber delivery of the pump power enables us to keep the laser resonator apart from the pump source, so that the laser resonator can be isolated from disturbances of the pump sources. In previous works, the high-order Hermite-Gaussian modes have been systematically generated by a fiber-coupled diode end-pumped Nd:yttrium-aluminum-garnet (YAG) laser [2,3]. The high-order Laguerre–Gaussian (LG) $TEM_{p,l}$ mode exhibits interesting physics and has the potential for technological applications, where p and l are the radial and azimuthal indices of the LG mode [4]. Recently, we developed a technique for the generation of the cylindrical symmetry LG modes with $p=0$ and specified values of l in a fiber-coupled diode end-pumped solid-state laser. The key novelty is to produce a doughnut-shaped pump profile by defocusing a standard fiber-coupled diode. The experimental results demonstrate that the stable transverse-mode pattern near the pump threshold is usually a LG $TEM_{0,l}$ mode with the distribution $\cos^2 l\phi$ (or $\sin^2 l\phi$) in azimuthal angle, having $2l$ nodes in azimuth. Even though the geometry is cylindrical symmetry, there is still certain astigmatism in the cavity due to the thermal lensing effect and anisotropic properties of the gain medium. This is the reason why sine or cosine LG modes, instead of doughnut modes, were generated near the pump threshold. A similar high-order LG $TEM_{0,l}$ mode has been reported in electrically pumped [5] and optically pumped [6] vertical-cavity surface-emitting semiconductor lasers (VCSEL's). However, the main difficulty of the emission of high-order LG modes in VCSEL's is that the processed wafer is in need of extraordinary homogeneity.

Slightly above the pump threshold in our laser setup, a LG $TEM^{*}_{0,l}$ or $TEM^{*}_{0,-l}$ mode, having a circle of constant intensity in the radial direction, can be generated by the superposition of two like $TEM_{0,l}$ modes, one rotated $\pi/2$ about the optical axis relative to the other. In recent years, the $TEM^{*}_{0,l}$ modes have attracted a great deal of interest in the mechanical and optical effects because they possess well-defined angular momentum along the optical axis when l is not zero [7]. These modes are also important in laser cooling and trapping experiment [8]. Therefore, it is of great interest to study the generation of the LG $TEM^{*}_{0,l}$ modes.

Astigmatism-induced splitting of the two like mode frequencies has a significant influence on laser dynamics. Temporal instabilities and chaotic emission caused by the nonlinear interaction of transverse modes in a class-A laser have been reported by Tamm [9] who experimentally confirmed the existence of ''cooperative frequency locking'' state [10] for the nearly degenerate $TEM_{0,1}$ and $TEM_{1,0}$ modes of a helium-neon laser. However, the dynamic characteristics of a solid-state laser are those of an oscillator with an inertial (noninstantaneous) nonlinearity. In the case of such oscillators the perturbations exhibit oscillatory relaxation. Because of relaxation oscillations, the two-mode locking in class-B laser occurs as a subcritical bifurcation [11–13], differently from class-A laser where the locking is a supercritical bifurcation. Not much has been done so far to observe this difference.

In this paper, we perform theoretical and experimental investigations of the relaxation oscillations in a LG $TEM^{*}_{0,l}$ mode solid-state laser for the standing-wave states and the traveling-wave states. Theoretical analysis shows that the relaxation oscillations play an important role not only in locking processes, but also under conditions of stationary states. On the other hand, a rich set of dynamical behaviors, such as periodic and quasiperiodic self-modulation, chaotic pulsing, and frequency locking, was experimentally observed in the generated $TEM^{*}_{0,l}$ hybrid mode. It was found that the experimental data exhibit a general satisfactory agreement with theoretical predictions.

*Author to whom correspondence should be addressed. FAX: (886-35) 729134. E-mail address: yfchen@cc.nctu.edu.tw

II. THEORETICAL ANALYSIS

A nonlinear system of the Maxwell-Bloch equations in terms of partial derivatives is usually reduced to a system of ordinary differential equations by expanding in terms of the empty-cavity modes for the laser system with a small number of excited transverse modes [12–15]. In this paper, we shall use this approach to study the dynamic instabilities in the two LG $\mathrm{TEM}_{0,l}$ modes in a class-B laser. To simplify the system of equations, we shall use the approximation of class-B lasers, i.e., $\gamma_\perp \gg \kappa, \gamma_\parallel$. Here $\gamma_\perp, \kappa, \gamma_\parallel$ are the decay constants of the polarization, and of the electromagnetic field, and of the population inversion, respectively.

When one longitudinal mode and the corresponding set of two like LG $\mathrm{TEM}_{0,l}$ modes are excited in a laser, the total optical field in a transverse cross section can be written as

$$E=\sqrt{\frac{2}{\pi l!}}\{\rho^1[(\cos l\phi)\Psi_c(t)\exp(-i\omega_c t) + (\sin l\phi)\Psi_s(t)\exp(-i\omega_s t)]\}\exp\left(-\frac{\rho^2}{2}\right)+\text{c.c.}, \quad (1)$$

where $\rho=\sqrt{2}r/w$; r is the polar radius, w is the beam radius, ϕ is the azimuthal angle, Ψ_c and Ψ_s are the amplitudes of the LG $\mathrm{TEM}_{0,l}$ cosine and sine modes, respectively, and ω_c and ω_s are the frequencies of the LG $\mathrm{TEM}_{0,l}$ cosine and sine modes. The exponential factors that govern the wave front curvature are omitted because they are unimportant for the present analysis. In the LG doughnut mode basis, expression (1) can be rewritten as

$$E=\sqrt{\frac{1}{2\pi l!}}\left\{\rho^1[\Psi_+(t)\exp(il\phi)+\Psi_-(t)\exp(-il\phi)] \times\exp\left[-i\frac{(\omega_c+\omega_s)t}{2}\right]\right\}\exp\left(-\frac{\rho^2}{2}\right)+\text{c.c.}, \quad (2)$$

where

$$\Psi_\pm=\Psi_c\exp\left(i\frac{\Omega t}{2}\right)\mp i\Psi_s\exp\left(-i\frac{\Omega t}{2}\right) \quad (3)$$

and

$$\Omega=\omega_c-\omega_s. \quad (4)$$

The LG modes with the amplitudes $\Psi_\pm$ are conveniently denoted by $\mathrm{TEM}^*_{0,l}$ and $\mathrm{TEM}^*_{0,-l}$. It can be easily demonstrated that there is a linear coupling between the $\mathrm{TEM}^*_{0,l}$ and $\mathrm{TEM}^*_{0,-l}$ modes because of astigmatism-induced splitting between the frequencies of the LG $\mathrm{TEM}_{0,l}$ cosine and sine modes. Using the Maxwell–Bloch system of equations and following the derivation of the previous works [15,16], we obtain the following system of equations:

$$\begin{aligned}
\frac{dF_+}{d\tau}&=(1-i\Delta)(F_+N_0+F_-N_2)+iR\exp(i\varphi)F_-,\\
\frac{dF_-}{d\tau}&=(1-i\Delta)(F_-N_0+F_+N_2^*)+iR\exp(i\varphi)F_+,\\
\frac{dN_0}{d\tau}&=1-\gamma N_0-|F_+|^2-|F_-|^2,\\
\frac{dN_2}{d\tau}&=-\gamma N_2-F_+F_-^*.
\end{aligned} \quad (5)$$

Here, the quantities $R\cos\varphi$ and $R\sin\varphi$ represent, respectively, the frequency difference and the loss difference of the $\mathrm{TEM}_{0,l}$ cosine and sine modes, such that if $\varphi=0$, then $R=\Omega/(2\sqrt{\gamma_\parallel\kappa\varepsilon})$; $F_\pm\rho^1\exp[\pm il\phi-(\rho^2/2)]$ are the amplitudes of the $\mathrm{TEM}^*_{0,\pm l}$, N_0 and N_2 are the zeroth and second angular harmonics of the population inversion described in Ref. [16], Δ is the dimensionless detuning from the line center in the absence of frequency splitting, $\gamma=\sqrt{\gamma_\parallel/(\kappa\varepsilon)}$, ε is the excess of the pumping rate above the threshold, normalized to κ, and τ is the dimensionless time. The system of Eq. (5) is similar to the system describing generation of counterpropagating wave (CPW) in a bidirectional ring class-B laser, as discussed in Refs. [17–19].

The vector field defined by Eq. (5) is invariant under the transform $F_\pm\rightarrow F_\pm\exp(i\theta)$, where θ is arbitrary constant. It is therefore convenient to introduce the new set of variables that are invariant under this transformation [16]:

$$\begin{aligned}
&x_0=N_0,\quad x_1=2\,\mathrm{Re}(N_2),\quad x_2=2\,\mathrm{Im}(N_2),\\
&x_3=|F_+||F_-|\cos\vartheta,\quad x_4=|F_4||F_-|\sin\vartheta,\\
&x_5=|F_+|^2-|F_-|^2,\quad x_6=|F_+|^2+|F_-|^2,\\
&\vartheta=\arg(F_+)-\arg(F_-).
\end{aligned} \quad (6)$$

In terms of the new set of variables, the system of Eq. (5) can be expressed in the form

$$\begin{aligned}
\dot{x}_0&=1-\gamma x_0-x_6,\\
\dot{x}_1&=-\gamma x_1-x_3,\\
\dot{x}_2&=-\gamma x_2+x_4,\\
\dot{x}_3&=-(2R\sin\varphi)x_6+x_6x_1+\Delta x_5x_2+2x_3x_0,\\
\dot{x}_4&=(2R\cos\varphi)x_5-x_6x_2+\Delta x_5x_1+2x_4x_0,\\
\dot{x}_5&=-(2R\cos\varphi)x_4+2x_5x_0-\Delta(x_4x_1+x_3x_2),\\
\dot{x}_6&=-(2R\sin\varphi)x_3+2x_6x_0-x_4x_2+x_3x_1.
\end{aligned} \quad (7)$$

In the following, we use Eq. (7) to simulate the behavior of the laser. This set of seven coupled nonlinear equations is numerically integrated using a fourth-order Runge-Kutta algorithm.

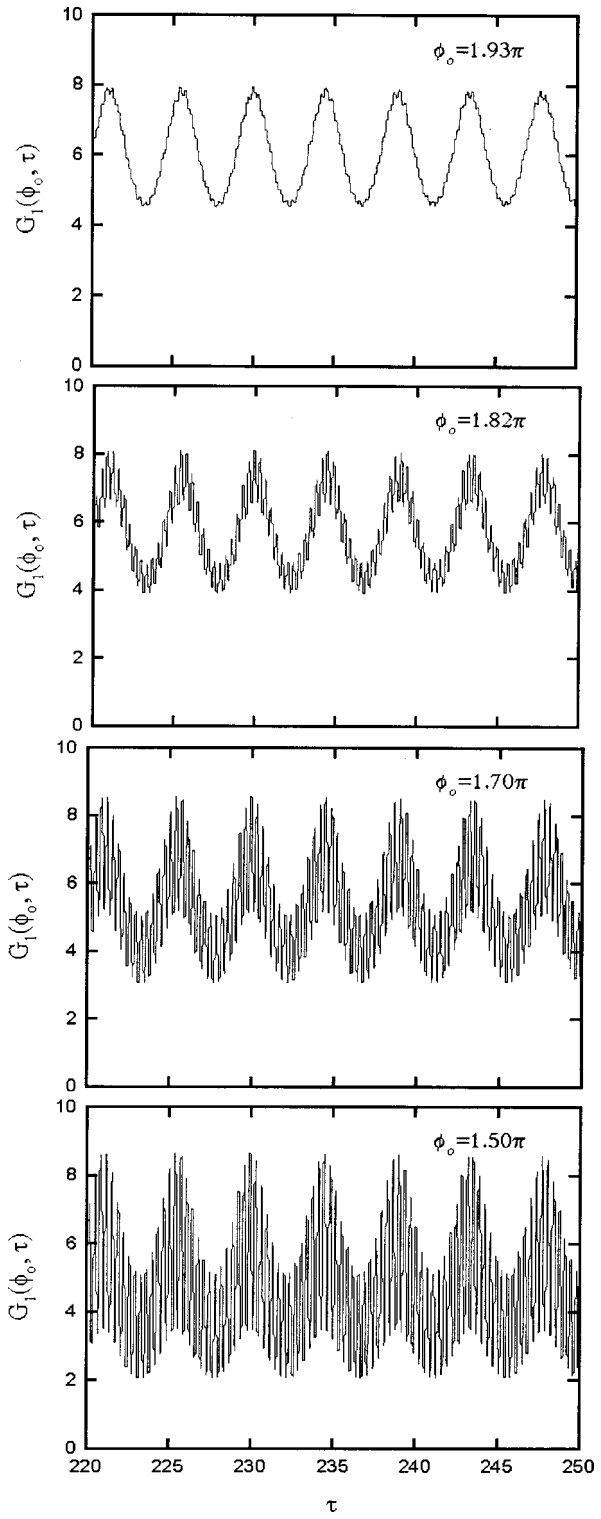

FIG. 1. Theoretical results obtained from the numerical calculations with $R=9.0$ and $\varphi=0$ for several detection angles for $l=1$ in the stable self-modulation regimes.

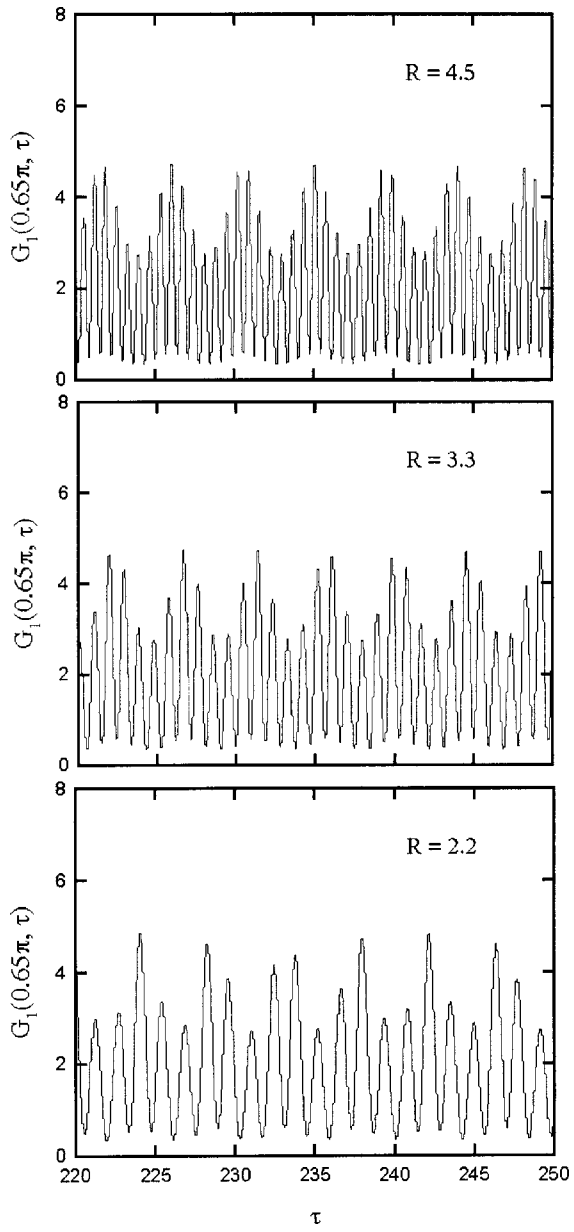

FIG. 2. Theoretical results obtained from the numerical calculations with $\varphi=0$ for several values of R for a fixed detection angle for $l=1$ in the stable self-modulation regimes.

We assume the frequency of the $TEM_{0,l}$ mode is in resonance with the frequency of a laser transition, i.e., $\Delta=0$. This allows for a simple demonstration for the dynamics of the LG $TEM^{*}_{0,\pm l}$ modes in a solid-state laser. At first we consider the steady-state solutions. A pair of solutions of the standing-wave type, corresponding to simultaneous generation of the $TEM^{*}_{0,\pm l}$ modes, is $|F_+|^2=|F_-|^2$. The total intensity of the radiation generated by a laser under these conditions is a LG $TEM_{0,l}$ mode with the distribution $\cos^2 l\phi$ (or $\sin^2 l\phi$) in azimuthal angle, having $2l$ nodes in azimuth. In addition, there are four traveling-wave solutions. A stable pair of traveling-wave solutions is $|F_+|\neq 0, |F_-|=0$ and, correspondingly, $|F_+|=0, |F_-|\neq 0$. They will be called the traveling waves TW_+ and TW_-, respectively. Another pair of traveling-wave solutions is $|F_+|>|F_-|$ and $|F_+|<|F_-|$, where $|F_\pm|\neq 0$; they will be called the traveling waves TW1 and TW2, respectively.

We investigated numerically the stability of the steady-state solutions. Typically, the parameter γ is very small in

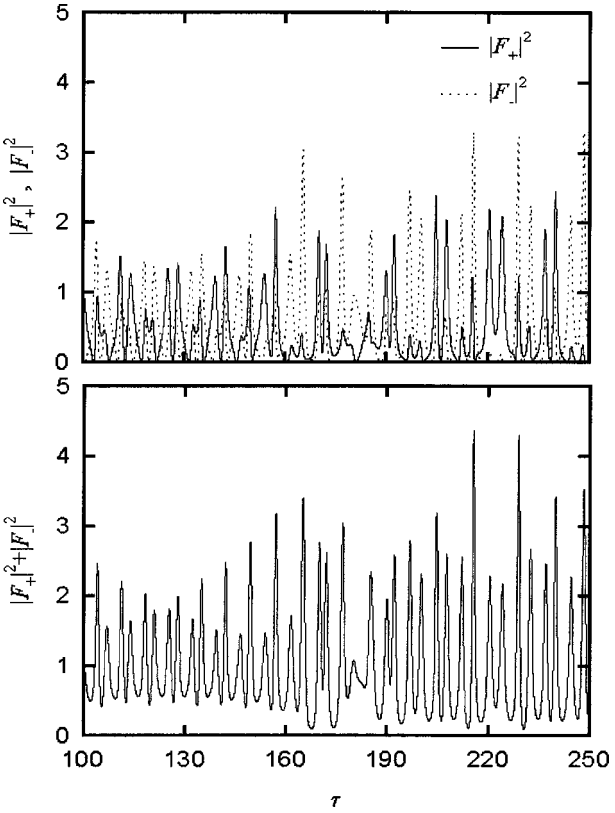

FIG. 3. Theoretical results obtained from the numerical calculation with $R=0.5$ and $\varphi=0$ for illustrating the chaotic oscillations.

class-B lasers. In the all calculations we used $\gamma=0.0033$ for our diode-pumped Nd:YVO4 laser in which $\gamma_{\parallel}\approx 10^4\,\mathrm{s}^{-1}$, $\kappa \approx 10^9\,\mathrm{s}^{-1}$, and $\varepsilon\approx 1.0$. The calculation results show that when the frequency difference $R\cos\varphi$ exceeds considerably the normalized relaxation frequency $\omega_r/(2\sqrt{\gamma_{\parallel}\kappa\varepsilon})$, i.e., $\Omega \gg \omega_r$, the solutions TW1 and TW2 exhibit stable relaxation oscillations modulated at the beat frequency. Here ω_r is the well-known relaxation frequency of a single-mode class-B

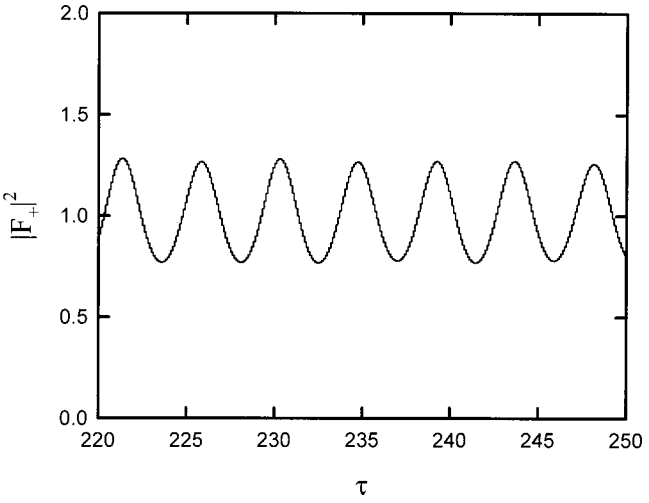

FIG. 4. Theoretical results obtained from the numerical calculation with $R=0.1$ and $\varphi=0$ for illustrating the frequency-locked state.

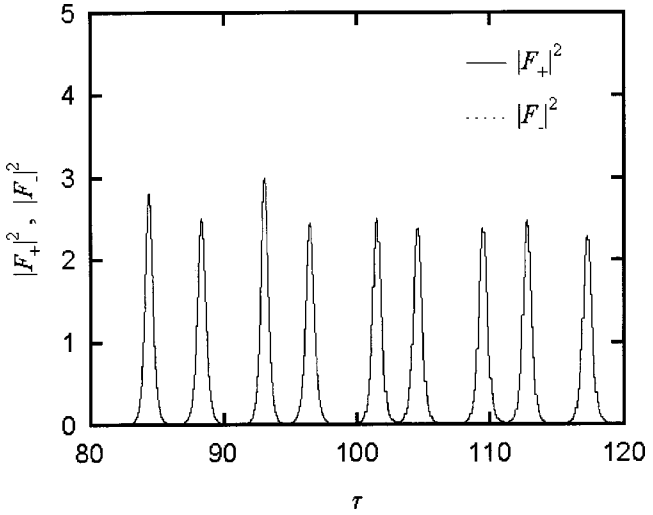

FIG. 5. Theoretical results obtained from the numerical calculation with $R=15$ and $\varphi=0$ for illustrating the self-pulsing oscillations.

laser: $\omega_r/\sqrt{\gamma_{\parallel}\kappa\varepsilon}=\sqrt{2-\gamma^2/4}$ [12,14,19]. The calculation results show that the intensities $|F_+|^2$ and $|F_-|^2$ are in antiphase at the modulation frequency (beat frequency), while they are in phase at the relaxation frequency; the total intensity $|F_+|^2+|F_-|^2$ exhibits pure relaxation oscillations. The intensity distribution in a transverse section of a $\mathrm{TEM}_{0,l}$ mode is given by

$$I(\rho,\phi,t)=\frac{1}{l!}\rho^{2l}\exp(-\rho^2)g_l(\phi,t), \tag{8}$$

where

$$g_l(\phi,t)=|F_+|^2+|F_-|^2+2|F_+||F_-|\cos(2l\phi+\vartheta). \tag{9}$$

Since $|F_+||F_-|\neq 0$ and the phase difference ϑ is a function of time for the self-modulation regimes, the modulation

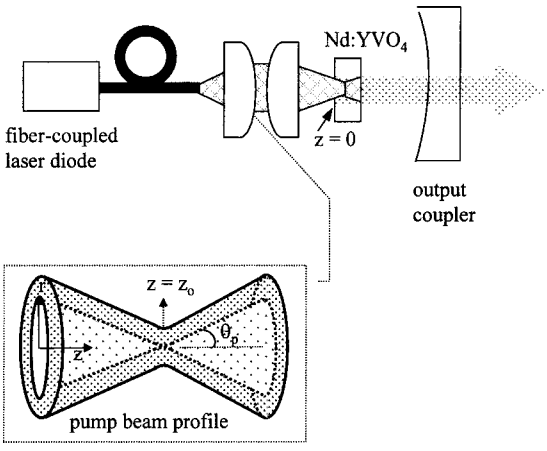

FIG. 6. Schematic of a fiber-coupled diode end-pumped laser; a typical beam profile of a fiber-coupled laser diode away from the focal plane.

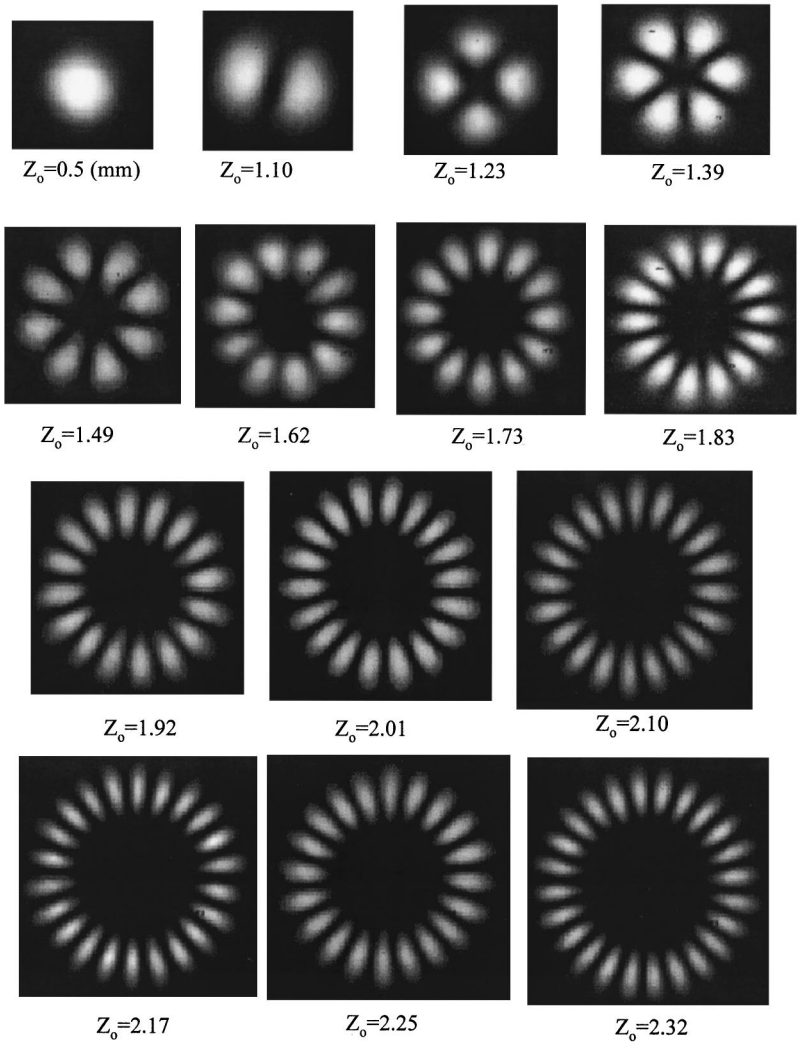

FIG. 7. Beam profiles with different LG TEM$_{0,l}$ mode distributions, measured with the CCD camera, in the 14 positions.

depth depends on the position. To demonstrate the spatiotemporal dynamics, we define the accumulative intensity as

$$G_l(\phi_o,t)=\int_0^{\phi_o} g_l(\phi,t)d\phi, \tag{10}$$

where ϕ_o represents the detection angle. Figure 1 shows a typical result obtained from the numerical calculation for $l=1$ with $R=9.0$ and $\varphi=0$. It can be seen that the modulation depth of the intensity strongly depends on the detection angle. Note that the modulation frequency will disappear in the total intensity $|F_+|^2+|F_-|^2$. Figure 2 shows the calculation results obtained with different values of R and $\varphi=0$ for a fixed detection angle in the self-modulation region. It can be found that the self-modulation is stable as long as the beat frequency exceeds considerably the relaxation frequency

In addition to the stable self-modulation regimes, the interaction between self-modulation and relaxation oscillations gives rise to the appearance of chaotic oscillations. The calculation results indicate that when the frequency difference $R\cos\varphi$ is between $\omega_r/(4\sqrt{\gamma_\parallel\kappa\varepsilon})$ and $\omega_r/(2\sqrt{\gamma_\parallel\kappa\varepsilon})$, i.e., $\omega_r/2<\Omega<\omega_r$, the intensities $|F_+|^2$, $|F_-|^2$, and the total intensity $|F_+|^2+|F_-|^2$ exhibits chaotic oscillations. One example illustrating the chaotic oscillations was shown in Fig. 3. The result was obtained from the numerical calculation with $R=0.5$ and $\varphi=0$. The analysis shows that the buildup of the relaxation oscillation is the mechanism of the appearance of dynamic chaos in LG TEM$^*_{0,\pm l}$ mode solid-state lasers. A similar self-stochastic regime was also studied numerically and observed experimentally in a self-contained solid-state ring laser [20].

When the frequency difference $R\cos\varphi$ is reduced below the critical value $\omega_r/(4\sqrt{\gamma_\parallel\kappa\varepsilon})$, i.e., $\Omega<\omega_r/2$, the self-modulation regime no longer exists; the solutions TW$_+$ and TW$_-$ are stable. The solutions TW$_+$ and TW$_-$ represent the frequency-locked transverse modes. In class-B lasers the locking occurs at a significantly smaller mode frequency difference, $\Omega<\omega_r/2$. Thus it is more difficult to obtain frequency locking in class-B than in class-A lasers. The relaxation oscillation plays an important role not only in transient processes, but also under conditions of steady operation of a solid-state laser (class-B laser). In the regime of frequency locking, the intensity exhibits relaxation oscillations, as shown in Fig. 4. Note that the time characteristic of the in-

tensity in the frequency-locking regime is independent of position because of $|F_+||F_-|=0$.

So far, the dynamics of the LG $\mathrm{TEM}^*_{0,\pm l}$ modes were discussed for the condition that the loss difference $R\sin\varphi$ is zero, i.e., $\varphi=0$. When the loss difference $R\sin\varphi$ is introduced in a class-B laser near the locking region, i.e., $\varphi\rightarrow\pi/2$, the total intensity exhibits a self-pulsing oscillation. Figure 5 depicts an example obtained from the numerical calculation with $R=15$ and $\varphi=\pi/2$. The numerical analysis shows that the total intensity under the self-pulsing region is nearly like a LG $\mathrm{TEM}_{0,l}$ mode with the distribution $\cos^2 l\phi$ (or $\sin^2 l\phi$) in azimuthal angle because $|F_+|^2\approx|F_-|^2$.

III. EXPERIMENTAL RESULTS

A. Experimental arrangement

Figure 6 shows the schematic of a fiber-coupled laser diode end-pumped Nd:YVO_4 laser considered in this paper. We used a plano-concave cavity that consists of one planar Nd:YVO_4 surface, high-reflection coated at 1064 nm and high-transmission coated at 809 nm for the pump light to enter the laser crystal, and a spherical output mirror. The second surface of the Nd:YVO_4 crystal (1 mm length) is antireflection coated at 1064 nm. A mirror with the reflectance of $R=97\%$ and the radius of curvature of 25 cm was used in the resonator to couple the output power. For a 1-cm resonator length, the waist of the fundamental mode was around 0.24 nm. The fiber-coupled laser diode (Coherent, F-81-800C-100) has a 0.1 mm of core diameter and was focused into the Nd:YVO_4 crystal by using a focusing lens with 0.57 magnification.

For a multimode fiber-coupled diode laser passing through a focusing lens, the profile at the focal plane is like a top-hat distribution; however, away from the focal plane it is like a doughnut-shaped distribution, as depicted in Fig. 6. With this property, we can defocus a standard fiber-coupled diode to result in a good overlap with the high-order LG $\mathrm{TEM}_{0,l}$ mode and generate it purely. From the characteristics of the pump beam profile, the radius of maximum pump intensity amplitude can be approximately described by $r_p(z)=\theta_p|z-z_o|$, where θ_p is the far-field half-angle, the point $z=0$ is taken to be at the incident surface of the gain medium, and z_o is the focal position of the pump beam in the laser crystal. The average radius of maximum pump intensity inside the gain medium, r_{pa}, is calculated by $\int_0^L r_p(z)e^{-\alpha z}\,dz/\int_0^L e^{-\alpha z}dz$, where α is the absorption coefficient at the pump wavelength and L is the length of the laser crystal. Carrying out the integration and using $e^{-\alpha L}\rightarrow 0$, the average radius of maximum pump intensity is given by $r_{pa}=\theta_p[z_o+(2e^{-\alpha z_1}-1)/\alpha]$.

For a single LG $\mathrm{TEM}_{0,l}$ mode, the normalized cavity mode distribution is given by

$$S_{0,l}(r,\phi,z)=\frac{4}{(1+\delta_{0,l})l!}\frac{1}{\pi\omega_o^2 L}(\cos^2 l\phi)\left(\frac{2r^2}{\omega_o^2}\right)^l \times\exp\left(-\frac{2r^2}{\omega_o^2}\right), \tag{11}$$

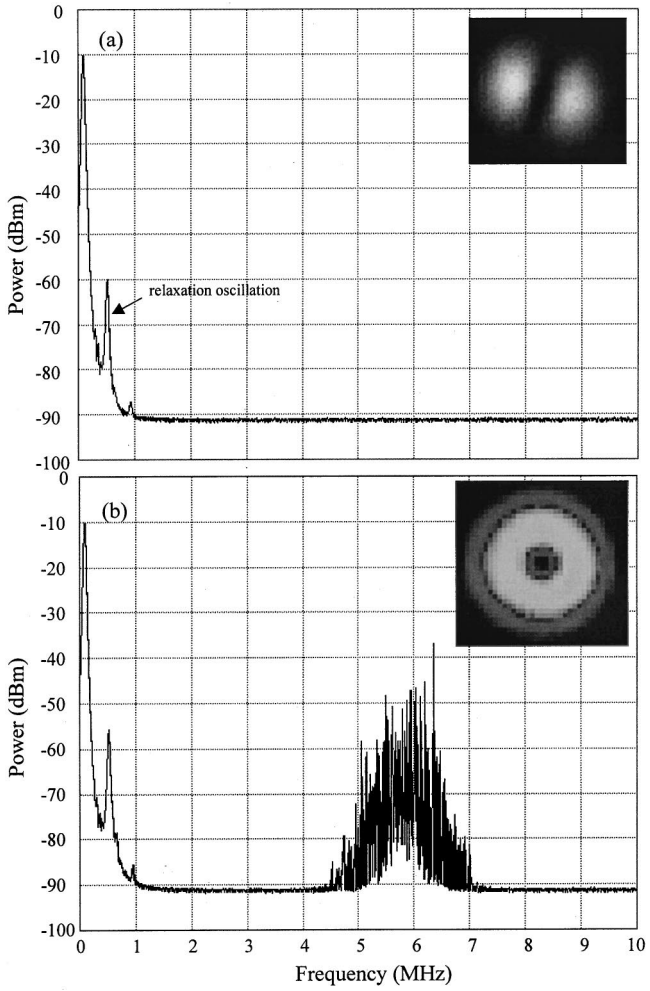

FIG. 8. (a) Power intensity spectrum of laser emission for one $\mathrm{TEM}_{0,l}$ mode. (b) Spectrum recorded when the laser simultaneously oscillates in the two first-order transverse modes, showing the mode-beating intensity modulation. Vertical scale: 10 dB/div; horizontal scale: 1 MHz/div.

where the z-dependent variation in $s_{0,l}(r,\phi,z)$ is neglected and the spot radii of the laser beam ω_o is approximated to be constant along the laser axis in the laser crystal. From Eq. (11), the radius of maximum mode intensity amplitude is trivially $r_{0,l}=\omega_o\sqrt{l/2}$. Since the cavity mode with the biggest overlap with the gain structure has the minimum threshold, we can obtain LG $\mathrm{TEM}_{0,l}$ mode output by adjusting the focal position z_o to achieve $r_{pa}=r_{0,l}$ for the best overlap. Figure 7 shows the experimental results for the output beam profiles with different transverse-mode distributions, measured with the charge-coupled device camera (Coherent, Beam-Code), in the 14 positions. The relation between transverse modes and pump positions is consistent with the prediction of pump-to-mode matching.

B. Dynamics of the $\mathrm{TEM}^*_{0,l}$ modes

Typically, the free-running one-mode class-B laser displays relaxation oscillations, as shown in Fig. 8(a). Relaxation oscillations play an important role in the dynamics of

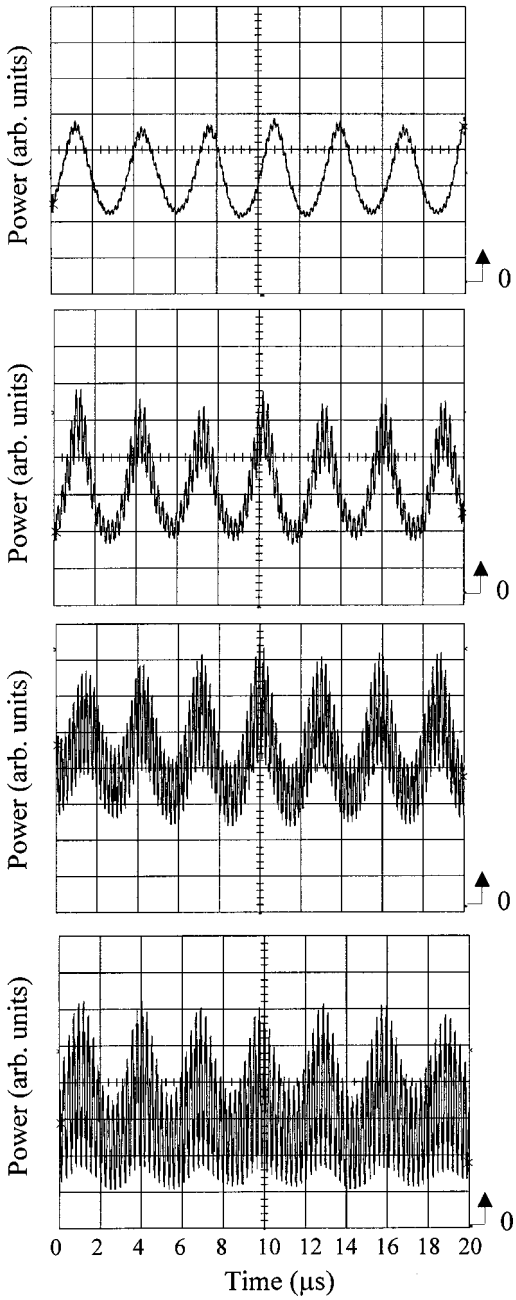

FIG. 9. Experimental results of the time characteristics for the stable self-modulation oscillations. Different modulation depths were obtained by changing the position of the detector.

two-mode class-B lasers. With a pump power slightly larger than the pump threshold, the laser operated in a LG $TEM^{*}_{0,l}$ doughnut mode that is a linear combination of two like $TEM_{0,l}$ modes, one rotated $\pi/2$ about the optical axis relative to the other. Since astigmatism lifts the degeneracy of the two like LG $TEM_{0,l}$ modes, a perfectly circular pattern is usually an ''unlocked doughnut'' as can be confirmed by observation of a beat signal shown in Fig. 8(b). The spatiotemporal dynamics of the unlocked doughnut could be observed by changing the position of the detector. It was found the modulation depth strongly depends on the position of the detector. Figure 9 shows the experimental results for

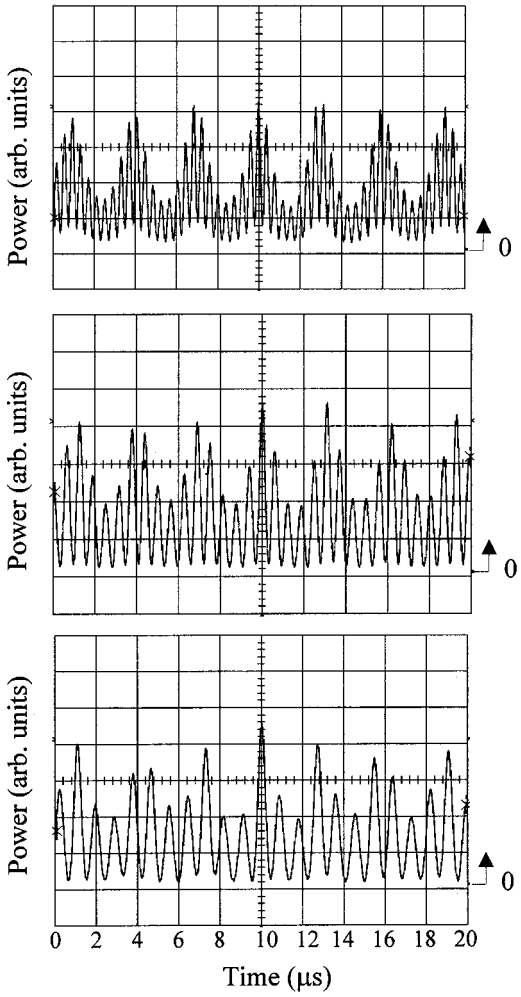

FIG. 10. Experimental results of the time characteristics for the stable self-modulation oscillations. Different modulation frequencies were obtained by slightly adjusting the output mirror.

different modulation depths observed in different positions. It is difficult to identify the relative position of the detector on the laser beam precisely because the detection area is very small. Even so, these results are in good agreement with the theoretical predictions shown in Fig. 1.

From the state of the perfectly circular pattern, the frequency difference between the two nearly degenerate modes can be decreased by a slight adjustment of the output coupler, as shown in Fig. 10. These results agree fairly well with the theoretical analysis presented in Fig. 2. Further decreasing the frequency difference, the appearance of chaotic generation regimes was observed, as shown in Fig. 11(a). This result confirms the fact that there is a chaotic set of solutions when the frequency difference is of the order of magnitude of the relaxation frequency, as depicted in Fig. 3. Decreasing the frequency difference smaller than the locking threshold, it eventually happens that the two likely modes lock to the same frequency, as shown in Figs. 11(b). We observed that the locking state has a strong tendency to jump to the states of chaotic pulsing by small perturbation. The bistable region of coexistence between locked and unlocked modes was observed, which confirms the fact that the locking in the

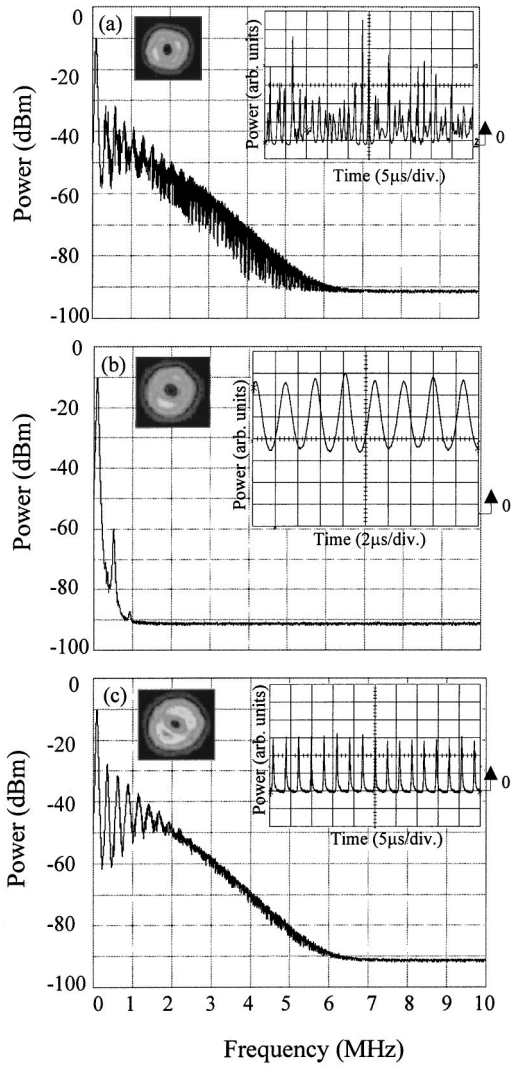

FIG. 11. (a) Power spectrum for the self-chaotic oscillations. (b) Power spectrum for the frequency-locked state. (c) Power spectrum for the self-pulsing oscillations. 1 MHz/div. Average transverse intensity distribution and time dependence are shown in the insets.

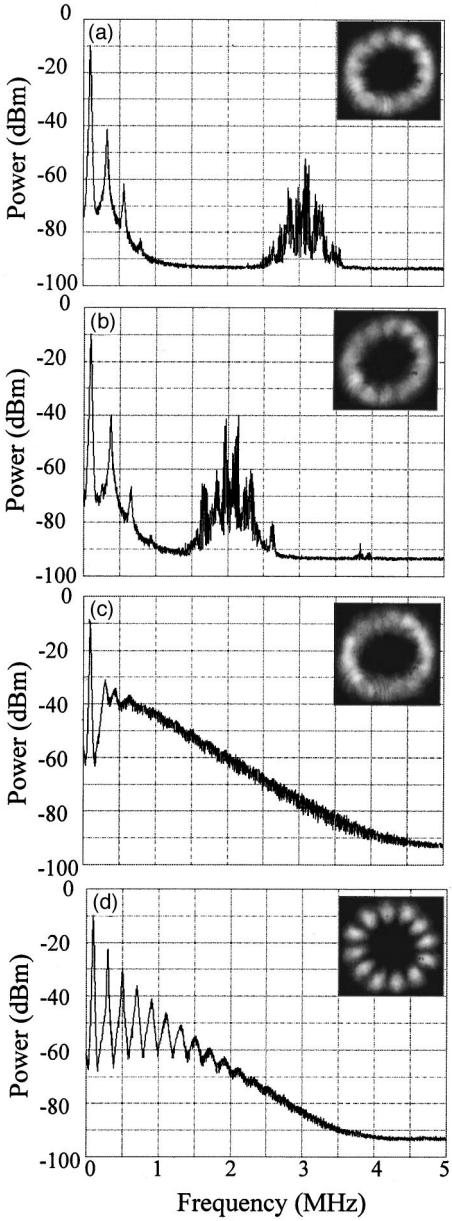

FIG. 12. Power spectra of laser emission for $TEM^*_{0,6}$ mode. Spectra (a)–(d) show the transition from self-modulation state (a) and (b) to chaotic pulsing (c) and the bifurcation of the locking to regular self-pulsing (d). Vertical scale: 10 dB/div; horizontal scale: 0.5 MHz/div.

class-B laser is a subcritical bifurcation, differently from class-A laser [11,12]. In the vicinity of the locking point, slightly adjusting the output coupler frequently may lead to a very stable regular self-pulsing operation of the laser, as shown in Fig. 11(c). Note that there are two obvious intensity maxima superposed on the background of the doughnut intensity distribution in the self-pulsing operation; this result indicates the loss difference between two like modes is significant. We also found that the regular self-pulsing state can hold for several hours, like a passively *Q*-switched laser. Besides, it is striking to notice that the repetition rate of the self-pulsing is slightly below the relaxation oscillation frequency. Moreover, we observed experimentally that the repetition rate increases with the pumping rate of the laser. These results definitely prove that this self-pulsed regime is due both to the frequency locking of the two nearly degenerate modes, and the existence of relaxation oscillations, i.e., to the fact that the population inversion cannot be eliminated adiabatically in class-B lasers [11,12]. Once again, the fact that the self-pulsed regime is experimentally obtained only in the vicinity of the locking point is consistent with the theoretical prediction. Furthermore, we also found a similar dynamical behavior like $TEM^*_{0,l}$ mode for other higher $TEM^*_{0,l}$ modes, as shown in Fig. 12.

Finally, it is worthwhile to mention that the present dynamics of transverse modes are strongly analogous to results obtained recently in the case of two polarization modes of a solid-state laser, in which Brunel *et al.* [21] observed similar dynamics, such as self-modulation, self-pulsing, and phase locking. Brunel *et al.* used two intracavity quarter-wave plates to result in a frequency difference between the *x* and *y* polarization directions; they used an uncoated silica etalon to

introduce a linear loss anisotropy. Similar to the present self-modulation regime, they found that when the loss difference is small and the frequency difference is slightly larger than the relaxation frequency of the laser, a usual beat note is observed between the two polarization modes. On the other hand, they also found that the introduction of a crossed loss anisotropy creating a locking region for two polarization states of a monomode solid-state laser leads to the self-pulsing regime. Similar to the present result, the self-pulsing behavior is physically attributed to the nonlinear interaction between two degenerate modes in the gain medium of lasers where the photon lifetime in the cavity is much shorter than the population inversion lifetime (class-B lasers). Moreover, Brunel *et al.* also found the phase locking between two polarization states in a solid-state laser to be a subcritical bifurcation. Although Brunel *et al.* did not investigate the chaotic regime sufficiently thoroughly, they were really aware of the existence of regions of chaotic behavior from preliminary theoretical and experimental observations.

IV. CONCLUSIONS

A detailed account has been given of self-modulation and relaxation oscillations in LG $TEM^*_{0,l}$ mode solid-state laser. The bifurcation mechanisms of excitation of self-modulation, chaotic, locking, and self-pulsing regimes have been investigated theoretically. It was found that the relaxation oscillation plays an important role not only in transient processes, but also under conditions of steady operation of a class-B laser. In addition, the buildup of the relaxation oscillation is the mechanism of the appearance of dynamic chaos in LG $TEM^*_{0,l}$ mode solid-state lasers. Furthermore, the introduction of a loss difference in the locking region has led to the self-pulsing regimes. From the observations of the locking phenomena of the first-order family, the experimental results agree very well with the theoretical predictions. It was also confirmed that the locking occurs as a subcritical bifurcation and a region of coexistence of locked and unlocked states exists.

ACKNOWLEDGMENT

The authors thank the National Science Council of the Republic of China for their financial support of this research under Contract No. NSC-89-2112-M-009-059.

[1] K. Otsuka, P. Mandel, and E. A. Viktorov, Phys. Rev. A **56**, 3226 (1997).
[2] H. Laabs and B. Ozygus, Opt. Laser Technol. **28**, 213 (1996).
[3] Y. F. Chen, T. M. Huang, C. F. Kao, C. L. Wang, and S. C. Wang, IEEE J. Quantum Electron. **33**, 1025 (1997).
[4] L. Dijaloshinski and M. Orenstein, Opt. Lett. **23**, 364 (1998).
[5] Q. Deng, H. Deng, and D. G. Deppe, Opt. Lett. **22**, 463 (1997).
[6] S. F. Pereira, M. B. Willemsen, M. P. Van Exter, and J. P. Woerdman, Appl. Phys. Lett. **73**, 2239 (1998).
[7] L. Allen, M. W. Beijersbergen, R. J. C. Spreeuw, and J. P. Woerdman, Phys. Rev. A **45**, 8185 (1992).
[8] J. W. Tabosa and D. V. Petrov, Phys. Rev. Lett. **83**, 4967 (1999).
[9] C. Tamm, Phys. Rev. A **38**, 3960 (1988).
[10] L. A. Lugiato, C. Oldano, and L. M. Narducci, J. Opt. Soc. Am. B **5**, 879 (1988).
[11] G. Slekys, C. O. Weiss, D. Y. Tang, and M. F. H. Tarroja, J. Opt. Soc. Am. B **11**, 2089 (1994).
[12] K. Staliunas, M. F. H. Tarroja, and C. O. Weiss, Opt. Commun. **102**, 69 (1993).
[13] F. Prati, L. Zucchetti, and G. Molteni, Phys. Rev. A **51**, 4093 (1995).
[14] M. Brambilla, M. Cattaneo, L. A. Lugiato, R. Pirovano, F. Prati, A. J. Kent, G. L. Oppo, A. B. Coates, C. O. Weiss, C. Green, E. J. D'Angelo, and J. R. Tredicce, Phys. Rev. A **49**, 1427 (1994).
[15] D. V. Skryabin, A. G. Vladimirov, and A. M. Radin, Quantum Electron. **27**, 892 (1997).
[16] A. G. Vladimirov and D. V. Skryabin, Quantum Electron. **27**, 887 (1997).
[17] P. A. Khandokhin and Ya. I. Khanin, J. Opt. Soc. Am. B **2**, 225 (1985).
[18] N. V. Kravtsov and E. G. Lariontsev, Quantum Electron. **24**, 841 (1994).
[19] A. G. Vladimirov, Opt. Commun. **149**, 67 (1998).
[20] P. A. Khandokhin and Ya. I. Khanin, Kvant. Elektron. (Moscow) **15**, 1993 (1998) [Sov. J. Quantum Electron. **18**, 1248 (1988)].
[21] M. Brunel, O. Emile, M. Alouini, A. L. Floch, and F. Bretenaker, Phys. Rev. A **59**, 831 (1999).